TEM study of NbC heterogeneous precipitation in ferrite

Fabien Perrard, Patricia Donnadieu, Alexis Deschamps, Patrick Barges

TEM study of NbC heterogeneous precipitation in ferrite

Journal:	*Philosophical Magazine & Philosophical Magazine Letters*
Manuscript ID:	TPHM-05-Jul-0350.R2
Journal Selection:	Philosophical Magazine
Date Submitted by the Author:	14-Nov-2005
Complete List of Authors:	Perrard, Fabien; LTPCM; Ascometal CREAS, Metallurgy Donnadieu, Patricia; LTPCM Deschamps, Alexis; LTPCM Barges, Patrick; Arcelor Research
Keywords:	transmission electron microscopy, precipitation, steel
Keywords (user supplied):	niobium carbide, heterogeneous precipitation

TEM study of NbC heterogeneous precipitation in ferrite

F. Perrard[1(+)], P. Donnadieu[1], A. Deschamps[1], P. Barges[2]

[1] LTPCM, CNRS UMR 5614, Institut National Polytechnique de Grenoble, Domaine Universitaire, BP75, 38402 St Martin d'Hères cedex, France

[2] Arcelor Research, Voie Romaine, BP30320, 57283 Maizières lès Metz, France

Abstract

The heterogeneous precipitation of NbC in ferrite has been quantitatively characterised by Transmission Electron Microscopy in a Fe-C-Nb model alloy for different isothermal heat treatments. Elongation and size distribution of precipitates have been derived from Dark Field imaging. For each precipitation states, the precipitation of NbC is occurring on dislocations due to the as-quenched state. This precipitation mechanism leads to characteristic arrays of precipitates in which precipitates grow in a self-similar manner. A detailed study of these arrays has shown that most dislocations decorated by these arrays are edge dislocations with <112> type line vectors. There is only one variant on a given dislocation. This selection can be interpreted by the interaction between dislocation and precipitate strain fields.

1. Introduction

The precipitation of Nb carbonitrides in ferrite is widely used in steels, especially for two main applications : for low solute contents (IF steels), the precipitation of NbC improves the drawability by removing C and N atoms out of solid solution [1] ; for higher solute contents (HSLA grades), the precipitation of Nb carbonitrides provides important precipitation hardening [2, 3].

Despite its high interest for the steel industry, the qualitative and quantitative characterization of NbC precipitation in ferrite remains incomplete. For instance the morphology and localization of precipitates are poorly documented in the early stages. In particular, the evolution of parameters such as precipitate mean radius and precipitate volume

(+) Present address: Ascometal CREAS, BP75045 57301 Hagondange cedex (France)

fraction during heat treatments has not been characterized in details. Two main reasons can be invoked for this lack of information. First most studies have been carried out on industrial alloys after complex thermomechanical heat treatments, and have focused on the relation between microstructure and mechanical properties [4]. In this case, it is difficult to know whether precipitates have nucleated in austenite, ferrite, or at the austenite / ferrite interface. Secondly, the very fine scale of NbC precipitation requires advanced characterization equipments, especially to get information on the first steps of the precipitation process.

According to the crystal structure of carbides, the Baker-Nutting relationship between ferrite and NbC precipitates is expected. However the NbC lattice parameter should lead to large misfits [5, 6]. Therefore, it is possible that heterogeneous precipitation occurs on grain boundaries or dislocations to release part of the elastic strain. Several studies have already shown some evidence of heterogeneous precipitation of NbC precipitation in ferrite [3, 7-9].

In this study, we have focused on the characterization of NbC precipitation in ferrite during isothermal heat treatments on a model Fe-Nb-C alloy using Transmission Electron Microscopy (TEM) to get on selected precipitation states the following information :

i.) morphology of precipitates together with quantitative data characterizing the precipitation state (aspect ratio, mean radius…);

ii.) localization of precipitates with a detailed study of their organization along dislocations.

In parallel with this TEM study, the entire precipitation kinetics have also been characterized by small angle neutron scattering (SANS) and will be published elsewhere [10].

2. Materials, heat treatments and experimental techniques

A high purity Fe-Nb-C alloy which composition is given in Table 1 has been studied. The alloy was prepared by vacuum induction melting, cast into ingots, and hot rolled from 50 mm to 5 mm thickness. After homogenization in the austenitic phase during 45 min at 1240°C and water quench, samples were heat treated at several temperatures and times. All samples were first heat treated in salt bath to ensure a reproducible heating rate. Longer ageing times (i.e. more than one hour) were obtained by heat treatments in silica tubes sealed under vacuum. Several samples have been predeformed by 10% cold rolling reduction before ageing in order to study the influence of a higher dislocation density on precipitation kinetics.

A Jeol 3010 microscope operating at 300kV was used to characterize the precipitation state for several heat treatments. Samples were mechanically thinned to 50µm and then electro polished in a Fischione double jet electropolishing device with a solution of 10ml water, 250ml glacial acetic acid, 75g anhydrous sodium chromate ($Na_2Cr_2O_7$) and 25g chromic oxide (CrO_3) [11], at 50V (45mA) for about ten minutes at room temperature. This solution delays the formation of surface oxides and improved the image quality compared to the classical acetoperchloric solution.

Precipitate size measurements were obtained by image analysis of Dark Field (DF) micrographs while the localization of precipitates was deduced from comparison between Dark Field (DF) and Bright Field (BF) images. The DF images were formed by selection of the $(002)_{NbC}$ spot. The disk shaped precipitates are then observed edge on which allows to measure both their long and short axis. Image analysis was only partially automatized. The particle selection was done manually because of the difficult thresholding on large areas. Using the image analysis software ImageTool parameters like long axis and short axis length, Feret radius, aspect ratio, and their respective distributions were obtained.

3. Qualitative characterization of the precipitation state

3.1. Morphology and crystallography of precipitates

Diffuse streaks consistent with disk shaped NbC carbides and located at positions consistent with a NaCl type structure and a Baker-Nutting relationship with the matrix are present on the diffraction patterns. These patterns will not be detailed here since others authors working on the same alloy within the CPR program have made a detailed TEM study including high resolution observations and have confirmed the disk shape as well as the composition and structure and orientation relationship of the NbC carbides [12]. The precipitate shape and structure observed on the present alloys are actually consistent with the literature on NbC precipitates in ferrite. The precipitates are then conveniently imaged by Dark Field imaging selecting the diffuse streak (for details see [3]). On such DF images which will be used in the following, the disk shaped precipitates are seen edge on.

Deleted: ¶
. . Figure 1a gives a [001] diffraction pattern on which the bright spots are indexed as Ferrite reflections while the diffuse one are due to the precipitates as well as pollution oxides. If NbC carbides with NaCl structure type (cfc, a_{NbC} =0.44 nm) and Baker-Nutting relationship ($(001)_{Fe}//(001)_{NbC}$ and $[110]_{Fe}//[100]_{NbC}$) are assumed, the NbC carbides are expected to be disk shaped and to display 3 variants in ferrite which generate spots on the [001] diffraction pattern as sketched in Figure 1b. Actually, diffuse spots consistent with NbC carbides having a NaCl type structure and a Baker-Nutting relation with the matrix are present on the diffraction patterns but they are difficult to observe because of the oxide pollution. ¶
. . ¶
. . On the DF image in Figure 1c, since the objective aperture was large enough to select several spots corresponding to NbC precipitates, several variants have been imaged, namely one variant laying in the observation plane (label 1 in Fig.1c) and two variants perpendicular to the observation plane (label 2 and 3 in Fig.1c). Note that the variant laying in the observation plane is visible only when precipitates are rather thick and when a large objective aperture is used. In further DF micrographs, only the disks seen edge-on will be imaged. The 3 variants indicate that the precipitates have an ellipsoid morphology, described by two long axis and a smaller one. These observations are consistent with a NaCl type structure for the NbC precipitates and a Baker-Nutting relationship.¶

3.2.Precipitation state after selected heat treatments

TEM has been carried out on the precipitation state corresponding to the heat treatments given in Table 2. For precipitate localization, comparison of BF and DF images was used. For DF imaging, the (200) $_{NbC}$ reflections were selected with a small objective aperture. To improve the contrast, the sample was tilted to get diffraction row condition along the (100) ferrite direction. Figure 1 to 3 show the precipitation state after ageing at 700 and 800°C for various times. In each case, the comparison between BF and DF micrographs clearly illustrates that most precipitates are located on dislocations. Besides, the precipitates form regularly spaced arrays along the dislocations. The precipitate sizes are on a nanometer scale, size characterization will be reported in details in the next section. As shown in Figure 3b precipitates are also present at the grain boundaries.

The precipitation state after predeformation and ageing for 300 minutes at 700°C (Figure 4) does not exhibit major differences with the sample aged for 300 minutes at 700°C but without prior predeformation. Figure 5 corresponds to a precipitation state obtained after 1000 minutes ageing at 600°C. In this state, precipitates are too small for a detailed study however they are obviously also regularly arranged along the dislocations.

To summarize, all the studied precipitation states exhibit a heterogeneous precipitation microstructure which is characterized by regular arrays of precipitates at the dislocations.

4. Quantitative characterization of the precipitation state

The precipitate size distribution has been measured by image analysis of DF micrographs for ageing states ranging from 300 and 3000 minutes at 700°C, 1 minute at 800°C without predeformation, and 300 minutes at 700°C after prior predeformation. In each case, about 1000 precipitates were analysed. We obtain the distributions of Feret radius (defined as the radius of a disk of equivalent area) and the average precipitate aspect ratio (defined as the ratio between the long and short axis), for the three ageing treatments. The radius distributions are given in Figure 6 and the characteristic values are gathered in Table 3.

As expected, the measurements in Figure 6 show an increase in precipitate average size with ageing time at 700°C. The ratio between the standard deviation and the average radius is observed to be constant (within the experimental precision) regardless of ageing

Deleted: 2
Deleted: 4
Deleted: 4b
Deleted: 5
Deleted: 6
Deleted: 7
Deleted: 7

temperature and time, indicating some self-similarity of the precipitate size distribution. The average aspect ratio lies between 2 and 2.5, and does not evolve much with heat treatments. It could be expected that for a given ageing state, the aspect ratio of precipitates is correlated with their size. To check this hypothesis, the aspect ratio has been plotted versus the long axis of precipitates in Figure 7. It appears that the correlation is very small; thus to a good approximation the average aspect ratio can be considered as characteristic of the whole precipitate distribution.

Deleted: 8

Precipitates in the sample with predeformation exhibit a slightly higher aspect ratio (3.0) compared to the other samples, whereas the mean radius is close to the values for the sample without predeformation. Except a slight effect on aspect ratio, the predeformation has no significant effect on the distribution. Actually the starting material was not free of dislocations; therefore even without deformation heterogeneous precipitation was already predominant. One further test has been done to check the heteogeneous character of precipitation since even if precipitates are on dislocations they can appear as if they were not on dislocations: The size distributions shown in Figure 6 are obtained considering all the precipitates on DF images. The distributions have been then re-evaluated taking in account only the precipitates which are obviously located at dislocations. We actually obtained the same mean radius for precipitates on dislocations compared to the measurement made with all precipitates. This validates the observation that most precipitates are situated on dislocations.

Deleted: 7

5. Heterogeneous precipitation

5.1.Study of the regular array of precipitates along dislocations

Concerning NbC precipitation at dislocations, the first point to clarify is whether or not several variants are present on a single dislocation. For DF micrographs taken with an objective aperture centered on the $\{200\}_{NbC}$ reflection, only one variant is imaged. Therefore DF imaging under two complementary conditions ($(200)_{NbC}$ and $(020)_{NbC}$) has been carried out on a same area. Figure 8 shows the BF image (Fig.8a) and the related DF images (Fig. 8b and 8c). It is obvious that only one variant is present on a given dislocation.

Deleted: 9
Deleted: 9a
Deleted: 9b
Deleted: 9c

On DF images, the precipitates on dislocations appear very regularly spaced. Besides, as illustrated by Figure 9, several typical alignment configurations are found. An interesting feature which should be measured from these arrays is the average precipitate density on the dislocations. However, TEM images being only projection of a 3D configuration, the true distance between precipitates can be derived only if one knows the dislocation line direction in 3D. Therefore, the point is now to identify the dislocation line direction and the related Burgers vector.

Identifying a dislocation line needs to take several images of a same area at different tilt angles. However the tilt possibilities on the microscope being limited to +/-30 °, and the samples being magnetic, the classical method appears to be not very efficient. Besides, the lines decorated by precipitates were quite straight which makes complex mixed dislocation rather unlikely. On the other hand, the character of dislocations in Ferrite is rather well documented. It can be then assumed that the dislocations are expected to be edge dislocations with ½ <111> Burgers vector and with line directions belonging to <110> or <112> types.

If we consider a TEM image taken for instance along the [0-11] zone axis, a limited number of projections have to be considered. Actually, owing to symmetry only two Burgers vectors can be considered : ½ [111] , vector laying in the projection plane (case 1), and ½ [-1-11] vector out of the projection plane (case 2). The stereographic projection can efficiently summarize the different cases since the projection plane and the set of possible lines directions for each Burgers vector can be reported. For instance, Figure 10, which corresponds to the case 2 (Burgers vector ½ [-1-11] out of projection plane), shows all the possible non equivalent configuration for dislocations lines as well as their projection on the TEM image. Besides, the stereographic projection allows also to estimate the angle of the projected line with respect to in plane crystallographic directions (for details see Fig.10 and its caption). If the DF images are obtained by selection of the $[200]_{NbC}$ reflection, the precipitates are seen edge on with their long axis direction in the projection plane ((0-11) here) perpendicular to the $[100]_{Fe}$ (=$[200]_{NbC}$) direction. It is therefore simple to derive the expected angle made by projected line and the precipitate normal, i.e. the $[100]_{Fe}$ (=$[200]_{NbC}$) direction (angle labelled 2 in Fig.10) or more conveniently, for comparison with Fig.10, the complementary angle 90°-angle 2 corresponding to the angle between the precipitate long axis and the projected line . Table 4 reports the expected projected line angles for case 2 (Burgers vector ½ [-1-11] out of projection plane). Note that for the in-projection plane ½

Deleted: 10

Deleted: 11

Deleted: 11

Deleted: 11

Deleted: 11

[111] Burgers vector, the projections are much simpler and therefore not shown in details here but this case was taken in account in our analysis (for details see [13]).

Actually with the help of the expected projection angles, the [0-11] zone axis DF image can be interpreted in terms of dislocation crystallography. The DF image in Figure 11 reports the dislocation line analysis obtained using the comparison of measured angles to the expected ones. Table 4 allows to interpret the typical projected configuration shown in Figure 9. Figure 9 b, d can be associated to <112> type dislocation lines and Figure 9 a, c to <110> type dislocation lines. According to Figure 11 and also to the most often observed configuration (Fig.9 b), and it comes out that the most frequent case corresponds to dislocations with a Burgers vector ½ [-1-11] and a [2-11] or [112] or [-121] line.

On DF images like Figure 11, it is also easy to check the validity of the edge dislocation hypothesis since there is no projection along direction corresponding to <111> type vectors as would be expected for screw dislocation.

The identification of the dislocation lines decorated with precipitates has been further used to derive the true distance between precipitates. For a 700°C, 300 min heat treatment, we obtained a 17 nm distance between precipitates along the dislocations, while for 700°C, 3000 min heat treatment, the distance between slightly increases to 20 nm. This information is of course of value for modelling the precipitation kinetics since it provides a direct measurement of the linear density of precipitates. It will be used in a forthcoming paper devoted to modelling of precipitation on dislocations.

5.2.Interaction between dislocations and precipitates

BF images of the dislocation have been carefully examined in order to consider the interaction between dislocation and precipitates. At high magnification, a dislocation decorated by precipitates (Fig.12a) appears not to have a straight direction but is rather forming a zig zag line as sketched by the insert in Figure 12a. Such behaviour is an indication for an interaction between the dislocation and precipitates. It has been also noticed that the contrast of dislocations is also strongly affected by the precipitates. This effect can be seen on the BF image in Figure 12a but also on the related DF images (Fig. 12b). One can note that as DF and BF images in Figure 12 were made with (100) $_{Fe}$ reflection under diffraction condition, a contrast should have been observed for any <111> Burgers vector. Besides, in

Deleted: 12
Deleted: 10
Deleted: 10
Deleted: 10
Deleted: 12
Deleted: 10
Deleted: 12
Deleted: 13a
Deleted: 13a
Deleted: 13a
Deleted: 13b
Deleted: figure
Deleted: 13

some cases, the comparison has been possible between a decorated dislocation to a precipitate-free dislocation. For instance, in Figure 1, there are several parallel dislocation lines: remarkably the decorated dislocations are almost out of contrast while the undecorated dislocations are contrasted. As the dislocation contrast is directly related to displacement field, such contrast extinction indicates that the precipitate and dislocations strongly interact through their displacement field.

Deleted: 2

The next step to better identify precisely the interaction between precipitates and dislocations is establish the relation between the dislocations and the selected variants. Indeed, it was found that only one variant of precipitates was present on a given dislocation. However, for one precipitate variant and one Burgers vector, several dislocation line vectors are possible (see section 5.1). As we only observe a projection of dislocations in the TEM image, it is not possible to go further in the identification of the line direction. Since the observations clearly indicate that there is a selection rule for one variant and that there is also an interaction of the precipitate and dislocation displacement field, the dislocation line possibilities have been further considered as well as their respective glide plane. If we consider one variant, for instance a precipitate with a disk normal parallel to $[100]_{Fe}$ and one type of Burgers vector, for instance ½ [-1-11], Table 5 gives the sets of possible dislocation lines and the corresponding glide plane. Remarkably, for a [100] precipitate variant, only the (011) glide plane contains the [100] direction. Hence though there are 3 possible equivalent possibilities for the dislocation, only one case corresponds to a displacement field with large components in a plane containing the precipitate disk normal. In other words, among the 3 possibilities, one can provide a better accommodation of the strain field due to the precipitate. If we assume such accommodation, it will mean in the case of interest here that, the [100] component of the dislocation displacement field is attenuated by the precipitate displacement field. Consequently, for a precipitate on a dislocation with a ½ [-1-11] Burgers vector, the resulting displacement field component will be mainly parallel to the [0-11] direction. It will then result that under (100) diffraction condition the decorated dislocation will have a weak contrast. Since this weak contrast has been observed, we propose that the selection of variant is controlled by the dislocation displacement field which contributes to reduce the elastic field due to the precipitate. Hence, as suggested earlier in the course of the precipitation study [14], the variant expected at a dislocation line corresponds to the one with a disk normal located in the dislocation glide plane.

6. Conclusion

The present TEM study has focused on the quantitative characterization of NbC carbides in Ferrite. For these nanometric disk shaped precipitates, we have derived from analysis of the DF images the size and aspect ratio distribution. Special interest was given to the precipitation on dislocations. Investigation of samples with or without predeformation and heat treated between 600 °C and 800°C shows that the precipitation is essentially heterogeneous. The precipitation along dislocations leads to characteristic arrays of precipitates. From a detailed study of these arrays, we identified the dislocation lines, derived the distance between precipitates and examined the interaction between dislocation and precipitates. The main points of this analysis can be summarized as follows :

i. a quantitative analysis of the precipitate size and aspect ratio shows that precipitates grow in a self-similar manner in the investigated conditions. The density of dislocations in an as-quenched material is sufficiently high so that most precipitates are located on dislocations in the undeformed material ; consequently a predeformation of the material before ageing does not significantly change the precipitate size and density.

ii. most dislocations decorated by precipitates are edge dislocations which line are of <112> type (although some <110> lines are also observed);

iii. only one variant of the NbC precipitates is present on a given dislocation. The variant selection is consistent with a precipitate/dislocation interaction which efficiently reduce the strain field due to the precipitates.

Acknowledgments

This work is part of a french scientific program (CPR Précipitation), in collaboration with Arcelor, Pechiney, CNRS, CEA, INPG, INSA Lyon, Université de Rouen, Université Aix-Marseille III and LEM-ONERA. T. Epicier and E. Courtois are gratefully acknowledged for fruitful discussions.

References

1.A. Jouet, *Les aciers hyperemboutissables pour l'industrie automobile.* La revue de métallurgie, **Novembre** p. 1425 (1997).

2.A.C. Kneissl, C.I. Garcia, and A.J. DeArdo. *Characterization of precipitates in HSLA steels*. Paper presented at the *HSLA steels : Processing, Properties and Applications*. (The Minerals, Metals and materials Society, 1992).

3.M. Charleux, W. Poole, M. Militzer*, et al.*, *Precipitation Behavior and its Effect on Strengthening of an HSLA-Nb/Ti Steel.* Metallurgical and Materials Transactions A, **32A** 7 p. 1635-1647 (2001).

4.T. Gladman, *The Physical Metallurgy of Microalloyed Steels*. (The Institute of Materials, London, 1997).

5.R.G. Baker and J. Nutting, *The tempering of a Cr-Mo-V-W and a Mo-V steel*, in *Precipitation processes in steels* (Iron and steel institute special report, London, 1959) p. 1-22.

6.A.J. DeArdo, J.M. Gray, and L. Meyer. *Fundamental metallurgy of niobium in steel*. Paper presented at the *International symposium Niobium*.San francisco, California. (TMS-AIME, 1984).

7.J. Bošanski, D.A. Porter, H. Åström*, et al.*, *The effect of stress annealing treatments on the structure of high heat-input welds containing Nb and Mo.* Scandinavian Journal of Metallurgy, **6** p. 125-131 (1977).

8.L.M. Perera, I.A. Rauf, J.D. Boyd*, et al. Precipitation and microstructural evolution in warm rolled Ti-Nb IF steel*. Paper presented at the *Advances in hot deformation textures and microstructures*. (The Minerals, Metals & Materials Society, 1994).

9.H.-J. Kestenbach, *Dispersion hardening by niobium carbonitride precipitation in ferrite.* Materials Science and Technology, **13** september p. 731-739 (1997).

10.F. Perrard, A. Deschamps, F. Bley*, et al.*, *Quantitative characterisation of fine scale precipitation kinetics in the Fe-Nb-C system.* (Submitted to Acta Mat.).

11.J.M. Rigsbee and H.I. Aaronson, *The interfacial structure of the braod faces of ferrite plates.* Acta Metallurgica, **27** p. 365-376 (1979).

12.E. Courtois, T. Epicier, and C. Scott, *Characterisation of niobium carbide and carbonitride evolution within ferrite: contribution of transmission electron microscopy and advanced associated techniques.* Materials Science Forum, **500-501** Nov p. 669-676 (2005).

13.F. Perrard, Caractérisation et modélisation de la précipitation du carbure de niobium et du cuivre dans les aciers bas carbone. PhD thesis, Institut National Polytechnique de

Grenoble (2004) available online at http://tel.ccsd.cnrs.fr/documents/archives0/00/00/70/78/index_fr.html.

14.T. Epicier, *communication at the Autrans meeting of the CPR " precipitation "*. 2003.

Figure captions:

Figure 1: Precipitation state after 1 minute at 800°C. The dark field (DF) image is taken using $(200)_{NbC}$ spot (elongated diffuse spots marked by an arrow in Fig 1a). In the following, precipates are always imaged with this DF condition. The comparison between BF and DF images highlights the precipitation of NbC along dislocations.

Figure 2: Precipitation state after 3000 min at 700°C. As for shorter heat treatment, comparing the BF and DF images indicates that the precipitates are located along dislocations.

Figure 3: Precipitation state after 300 min at 700°C. According to BF and DF images, the precipitation occurs along dislocations (upper part of the micrographs) and also grain boundaries (bottom part).

Figure 4: Microstructure of a 10% predeformed sample after ageing at 700°C for 300 min. As for the undeformed states, precipitation occurs along dislocations.

Figure 5: Microstructure after 1000 min at 600°C. As for higher ageing temperatures, precipitates are found along dislocations.

Figure 6: Feret radius distribution and characteristic values determined by TEM for four precipitation states.

Figure 7: Aspect ratio vs. long axis length of precipitates for the four studied precipitation states. Weak correlation exists between these two parameters.

Figure 8: Location of precipitates in a sample aged for 300 minutes at 700°C, after 10% predeformation. For a same area, the BF image (Fig. 8a) and two DF images (Fig. 8b, 8c) have been recorded. Each DF image is formed using two spots allowing to see different precipitate variants : $(200)_{NbC}$ and $(020)_{NbC}$. Comparison of the BF and DF images shows that only one type of variant is found at a dislocation line.

Deleted: Figure 1: Diffraction pattern under $[001]_{\alpha}$ zone axis with the corresponding spot indexation and DF image using $(200)_{NbC}$ spot with a large objective aperture. Figure 1c shows the three variants and the plate-like shape of NbC precipitates.

Deleted: 2

Deleted: 2a

Deleted: 3

Deleted: 4

Deleted: 5

Deleted: 6

Deleted: 7

Deleted: 8

Deleted: 9

Deleted: 9a

Deleted: 9b

Deleted: 9c

Figure 9: Typical configurations observed for precipitates along dislocation lines for imaging conditions as in Figure 1. In a (110) observation plane, the angles between precipitate major axis and projected dislocation lines take some particular values : ~ 0° (Fig 9a); ~ 30° (Fig 9b) ; ~ 50° (Fig 9c); ~ 90° (Fig 9d); Fig 9b corresponds to the most frequent case.

Figure 10: Stereographic projection representing case 2: Burgers vector out of the negative plane. The projection allows to represent interesting directions and planes: Burgers vector (B), possible dislocation lines, zone axis (A) corresponding to the negative and the planes normal to these directions: plane normal to A (i.e. the negative plane), plane normal to B which, for edge dislocation, contains the dislocations lines. Using the stereographic projection, some angles can be simply derived: angle labelled 1 between the dislocation line and the projected line, angle labelled 2 between the projected dislocation line and the [100] direction in the negative plane. Here in the chosen DF imaging condition, the [100] direction corresponds the normal to the observed precipitate major axis direction.

Figure 11: Example of alignments observed for High Nb alloy after 3000 minutes at 700°C the zone axis is close to [0-11]. On TEM image, with the help of the diffraction pattern, the direction of the projected lines can be approximately indexed and we can also measured the angle between the precipitate axis and the projected dislocation lines. Comparing these data to Table 4 allows to identify the dislocation line corresponding to the projection on Fig. 11. The longest precipitate alignments ([-355] projected direction) correspond to <112> type dislocation lines.

Figure 12: Interaction between precipitates and dislocation in a sample aged 3000 minutes at 700°C. Note that the precipitates are quite regularly spaced and the dislocation has a rather zig zag. This effect can be seen on the BF image in Fig. 12a and on the DF image in Fig. 12b. For DF imaging, a (200) Fe spot was selected to examine the dislocation contrast. Remarkably the dislocation contrast between precipitates is quite weak which indicate that the precipitates reduce the dislocation strain field.

Deleted: 10
Deleted: 2
Deleted: 10a
Deleted: 10b
Deleted: 10c
Deleted: 10d
Deleted: 10b
Deleted: 11
Deleted: 12
Deleted: 12
Deleted: 13:
Deleted: 13a
Deleted: 13b

Tables

Nb	C	N	S	P	Al	O
790	110	10	23	10	60	13

Table 1: Chemical composition (weight ppm).

Temperature (°C)	Time (min)	Predeformation prior to ageing
800	1	No

700	3000	No
700	300	No
700	300	Yes
600	1000	No

Table 2: Precipitation states observed in this study.

Precipitation state	R_{Feret} (nm)	σ (nm)	σ/ R_{Feret}	Aspect ratio
1 minute at 800°C	1.6	0.47	0.29	2.2
3000 minutes at 700°C	2.3	0.75	0.33	2.4
300 minutes at 700°C	1.8	0.58	0.32	2.3
300 minutes at 700°C, after 10% prior predeformation	1.7	0.48	0.28	3.0

Table 3: quantitative results obtained by TEM after image analysis

Dislocation lines	Projection on the negative (*)	Projection Angle	Angle between projected lines and (100) (angle 1 - Fig.10)	Angle between precipitate axis and projected lines (90° - angle 2)
$[2\bar{1}1]$	[100]	45°	0°	90°
[101]	[211]	30°	35°	55°
[112]	[355]	20°	67°	23°
[011]	[011]	0°	90°	0°
$[\bar{1}21]$	$[\bar{3}55]$	20°	123°	23°
$[\bar{1}10]$	$[\bar{2}11]$	30°	145°	55°

Table 4: Summary of stereographic projection results for case n°2. (*) Some projected line directions are in some cases approached ones.

Imaging diffraction condition : Row condition along $(100)_{Fe}$ direction, DF with (100) NbC reflection : Precipitate variant (disk normal) [100]			
Dislocation line for b= ½ [-1-11]	[2-11]	[112]	[-121]
Glide plane for b= ½ [-1-11]	(011)	(-110)	(101)

Table 5: Possible dislocation lines and corresponding glide planes for the specific condition where the precipitate normal is parallel to $[100]_{Fe}$. Among the glide plane possibility, only one contains the direction normal to the precipitate disk: here the (011) plane which is contains the [100] direction.

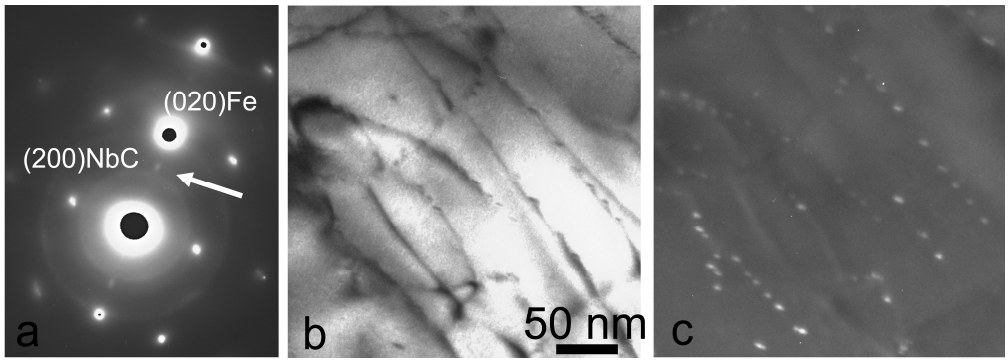

Precipitation state after 1 minute at 800°C. The dark field (DF) image is taken using (200)NbC spot (elongated diffuse spots marked by an arrow in Fig.1a). In the following, precipates are always imaged with this DF condition. The comparison between BF and DF images highlights the precipitation of NbC along dislocations.
199x70mm (600 x 600 DPI)

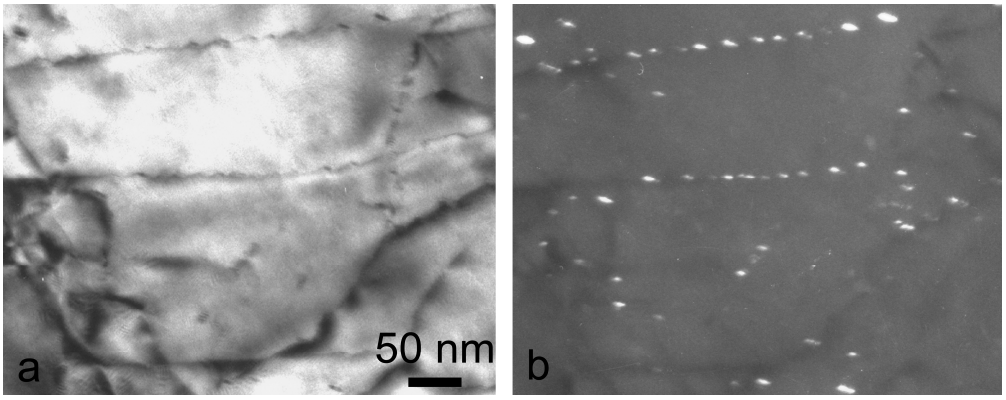

Precipitation state after 3000 min at 700°C. As for shorter heat treatment, comparing the BF and DF images indicates that the precipitates are located along dislocations.
199x78mm (600 x 600 DPI)

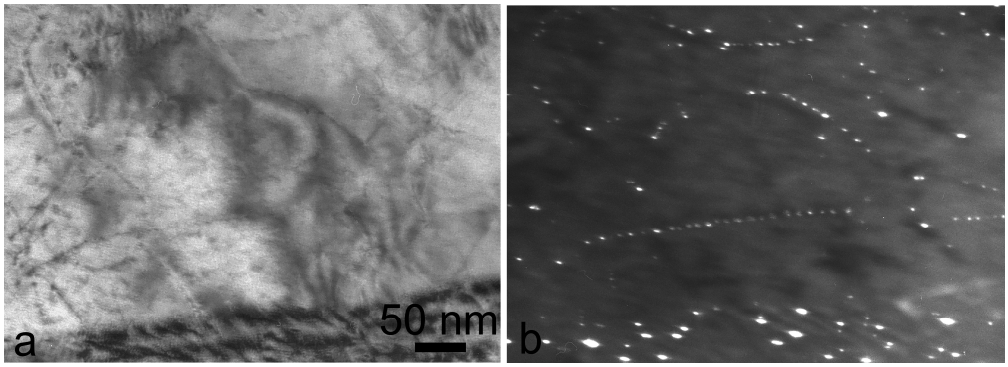

Precipitation state after 300 min at 700°C. According to BF and DF images, the precipitation occurs along dislocations (upper part of the micrographs) and also grain boundaries (bottom part).
199x71mm (600 x 600 DPI)

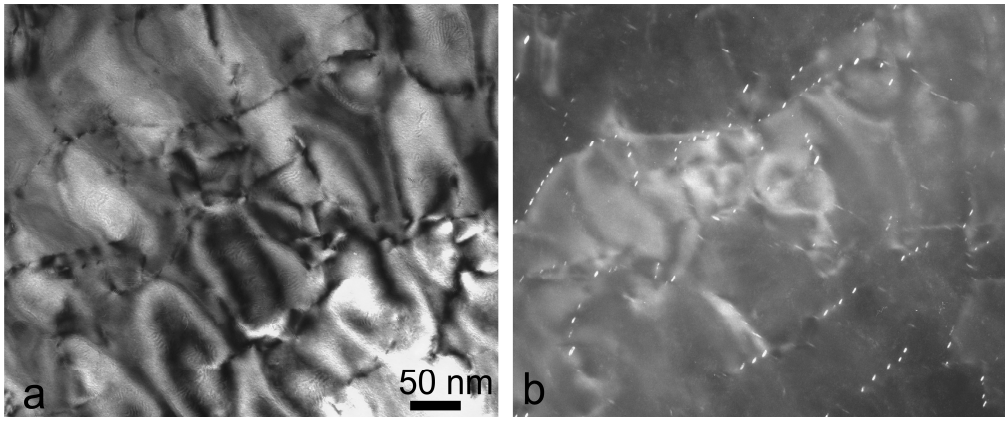

Microstructure of a 10% predeformed sample after ageing at 700°C for 300 min. As for the undeformed states, precipitation occurs along dislocations.
199x82mm (600 x 600 DPI)

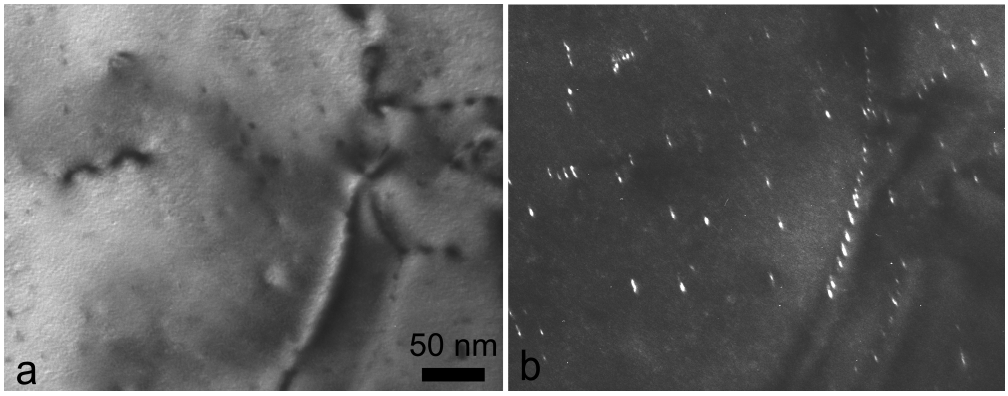

Microstructure after 1000 min at 600°C. As for higher ageing temperatures, precipitates are found along dislocations.
199x77mm (600 x 600 DPI)

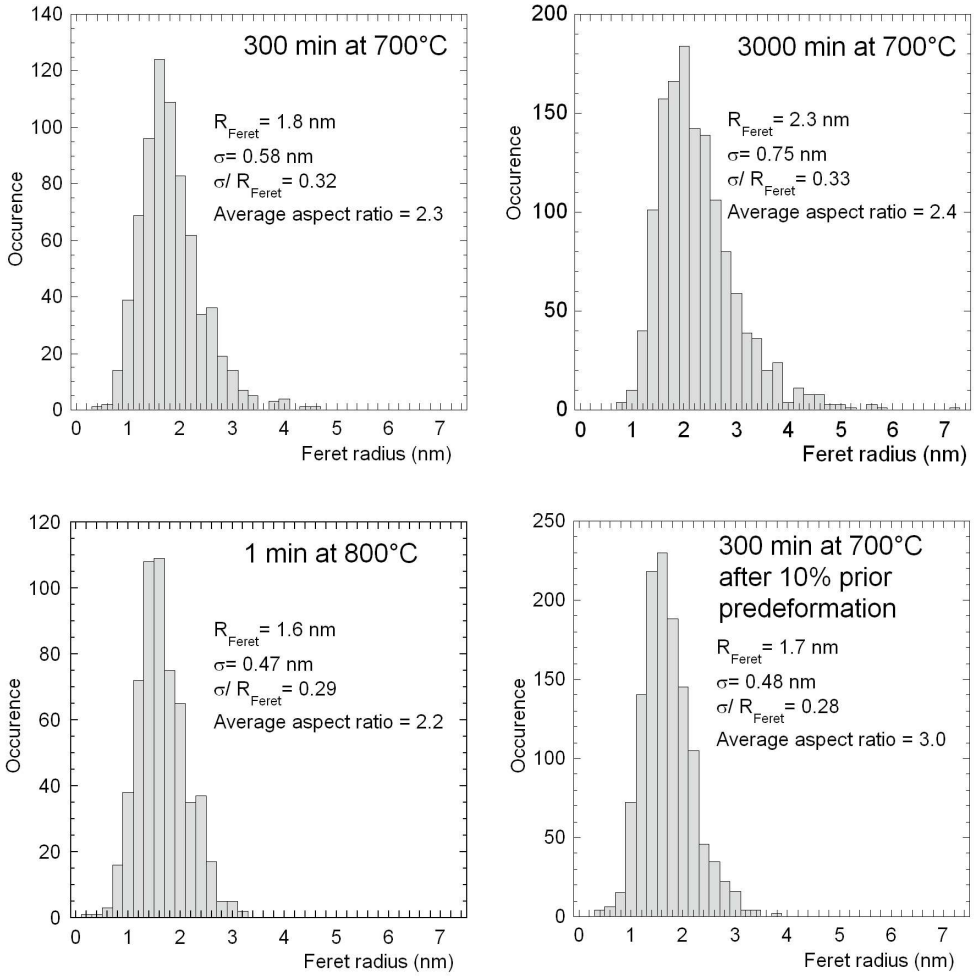

Feret radius distribution and characteristic values determined by TEM for four precipitation states.
160x165mm (288 x 288 DPI)

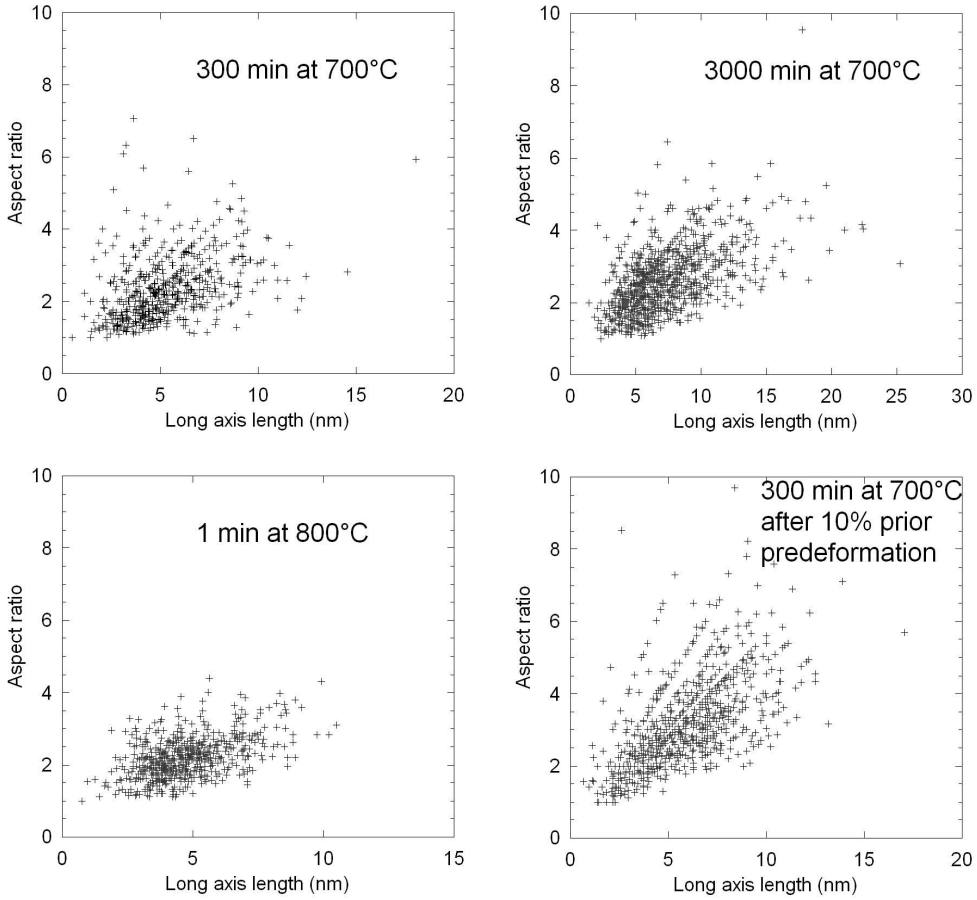

Elongation vs. long axis length of precipitates for the four studied precipitation states. Weak correlation exists between these two parameters.
162x163mm (288 x 288 DPI)

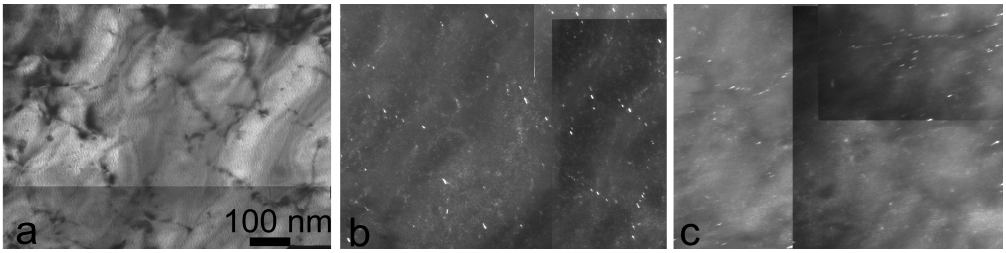

Precipitates localization in a sample aged for 300 minutes at 700°C, after 10% predeformation. For a same area, the BF image (Fig. 8a) and two DF images (Fig. 8b, 8c) have been recorded. Each DF image is formed using two spots allowing to see different precipitate variants : (200)NbC and (020)NbC. Comparison of the BF and DF images shows that only one type of variant is found at a dislocation line.
199x49mm (600 x 600 DPI)

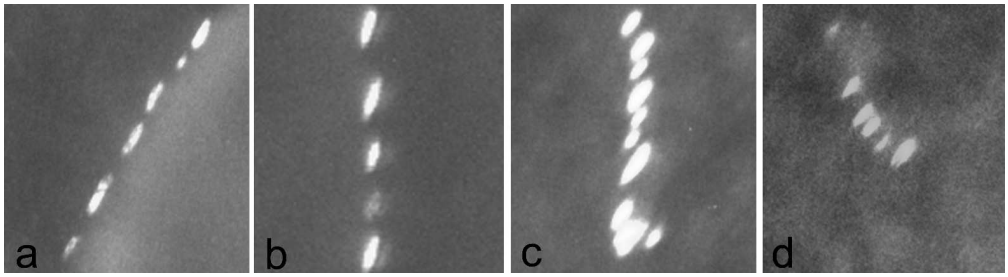

Typical configurations observed for precipitates along dislocation lines for imaging conditions as in Figure 1. In a (110) observation plane, the angles between precipitate major axis and projected dislocation lines take some particular values : ~ 0° (Fig 9a); ~ 30° (Fig 9b) ; ~ 50° (Fig 9c); ~ 90° (Fig 9d); Fig.9b corresponds to the most frequent case.
199x53mm (600 x 600 DPI)

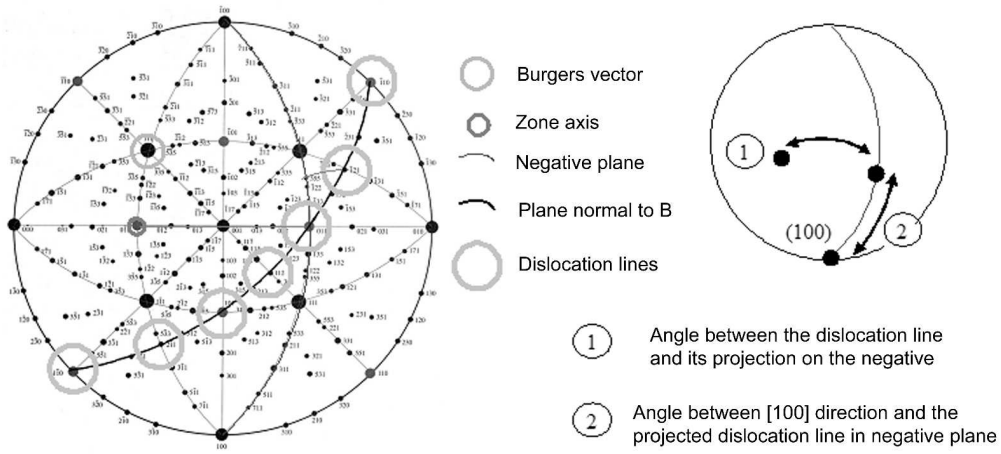

Stereographic projection representing case 2: Burgers vector out of the negative plane. The projection allows to represent interesting directions and planes: Burgers vector (B), possible dislocation lines, zone axis (A) corresponding to the negative and the planes normal to these directions: plane normal to A (i.e. the negative plane), plane normal to B which, for edge dislocation, contains the dislocations lines. Using the stereographic projection, some angles can be simply derived: angle labelled 1 between the dislocation line and the projected line, angle labelled 2 between the projected dislocation line and the [100] direction in the negative plane. Here in the chosen DF imaging condition, the [100] direction corresponds the normal to the observed precipitate major axis direction.
199x91mm (600 x 600 DPI)

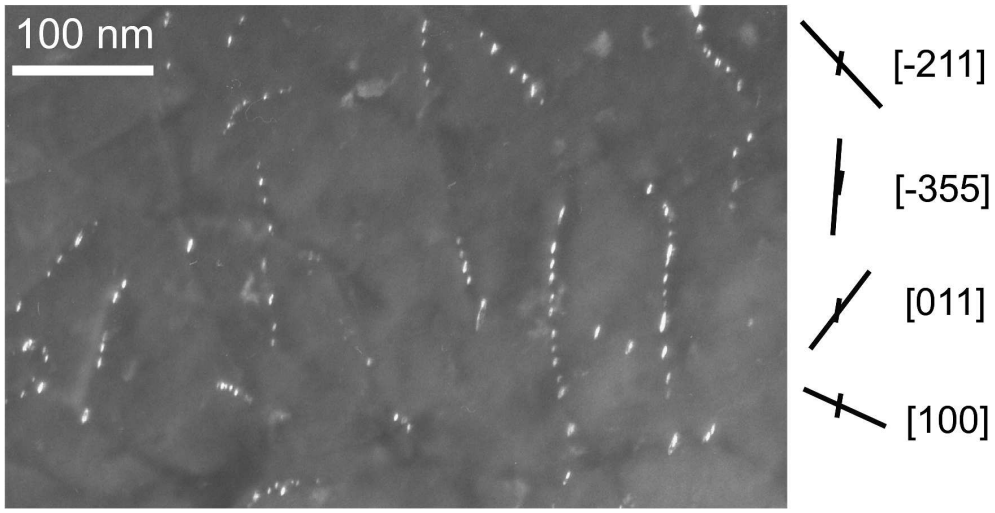

Example of alignments observed for High Nb alloy after 3000 minutes at 700°C the zone axis is close to [0-11]. On TEM image, with the help of the diffraction pattern, the direction of the projected lines can be approximately indexed and we can also measured the angle between the precipitate axis and the projected dislocation lines. Comparing these data to Table 4 allows to identify the dislocation line corresponding to the projection on Fig. 11. The longest precipitate alignments ([-355] projected direction) correspond to <112> type dislocation lines.
179x90mm (500 x 500 DPI)

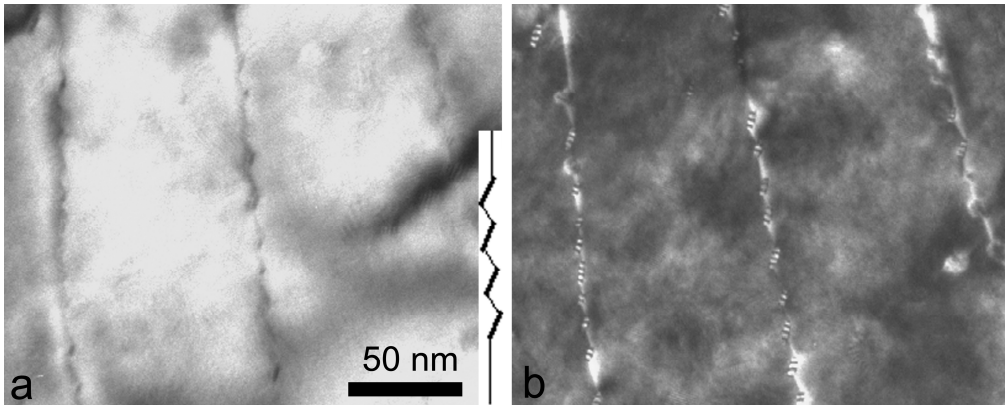

Interaction between precipitates and dislocation in a sample aged 3000 minutes at 700°C. Note that the precipitates are quite regularly spaced and the dislocation has a rather zig zag. This effect can be seen on the BF image in Fig. 12a and on the DF image in Fig. 12b. For DF imaging, a (200) Fe spot was selected to examine the dislocation contrast. Remarkably the dislocation contrast between precipitates is quite weak which indicate that the precipitates reduce the dislocation strain field.
199x80mm (600 x 600 DPI)